

During and After Solidification Using Real-Time Measurements

HOSSEIN MEHRARA, DMITRY G. ESKIN, ROUMEN H. PETROV,
MEHDI LALPOOR, and LAURENS KATGERMAN

A technique for measuring the linear contraction during and after solidification of low-alloy steel was developed and used for examination of two commercial low-carbon and low-alloy steels. The effects of several experimental parameters on the contraction were studied. The solidification contraction behavior was described using the concept of rigidity in a solidifying alloy, evolution of the solid fraction, and the microstructure development during solidification. A correlation between the linear contraction properties in the solidification range and the hot crack susceptibility was proposed and used for the estimation of hot cracking susceptibility for two studied alloys and verified with the real casting practice. The technique allows estimation of the contraction coefficient of commercial steels in a wide range of temperatures and could be helpful for computer simulation and process optimization during continuous casting.

DOI: 10.1007/s11661-013-2089-9

© The Minerals, Metals & Materials Society and ASM International 2013

I. INTRODUCTION

THE continuous casting (CC) process is the most common route to produce primary and semi-finished steel products for subsequent processing. Although the process has been continually improved since its emergence, the ongoing increase in casting speeds and demanding dimensions of slabs still causes casting defects such as uneven shell growth, surface marks, surface and internal cracks and breakouts to mention but a few. The CC process involves complicated phenomena like heat and mass transport, solidification and shell formation, structure development, evolution of thermophysical and thermomechanical properties, etc., a better understanding of which are essential for treating those defects and increasing productivity of the CC technology.^[1–3]

Hot cracking is one of the prevalent problems in CC practice of low-carbon and low-alloy steels. It forms when stresses and strains built up during solidification exceed strength and ductility developed in the solidifying material. It is well accepted that such conditions are most likely to occur at high solid fractions where solid grains have essentially formed a *coherent* dendritic network capable

of transferring stresses but films of liquid still remain at grain boundaries, thereby weakening the material and making it vulnerable to cracking if the material is exposed to tension.^[4] A systematic treatment of the crack formation process requires knowledge of structure formation within the solidification range, mushy zone coherency, and rigidity, solidification shrinkage, feeding of growing solid along with its thermal contraction, which are all interrelated phenomena.

The term “coherency” has not been always used in the same meaning by researchers through hot cracking studies. The obtained values of coherency temperature and fraction solid depend on the type of testing and on grain structure.^[5] In the context of solidification shrinkage and contraction testing, terminology used in literature to describe structure and mechanical behavior of mushy zone is mostly suited for equiaxed and mixed morphologies—usually observed in aluminum alloys.^[6–8] However, the microstructure is predominantly columnar dendritic during initial solidification inside a CC mold just below the meniscus.^[9] Thus, to avoid ambiguity arising from morphology-related physical and mechanical behavior of a solidifying shell, it is worthwhile to specify some features of the mushy zone with the columnar dendritic morphology.

The complex mechanics of the solidifying shell (including the mushy zone being in constant contact with a growing solid layer) can be attributed to its structure composed of multiple regions; each with different morphologies and mechanical responses to a transverse tension,^[10] i.e.,

- region of easy feeding;
- region of restricted interdendritic flow due to densification of dendritic network and liquid film formation;
- region of liquid droplets in the grains and liquid films/pockets at the grain boundaries;

HOSSEIN MEHRARA, Ph.D. Student, and MEHDI LALPOOR, Postdoctoral Researcher, are with the Materials Innovation Institute, Delft, The Netherlands and also with the Department of Materials Science and Engineering, Delft University of Technology, Delft, The Netherlands. DMITRY G. ESKIN, Professor, is with the Brunel Centre for Advanced Solidification Technology, Brunel University, Uxbridge, U.K. Contact e-mail: Dmitry.eskin@brunel.ac.uk ROUMEN H. PETROV, Associate Professor, is with the Department of Materials Science and Engineering, Delft University of Technology and also with the Department of Materials Science and Engineering, Gent University, Gent, Belgium. LAURENS KATGERMAN, Professor, is with the Department of Materials Science and Engineering, Delft University of Technology.

Manuscript submitted May 21, 2013.



82 (d) region of liquid droplets in the grains and at the
83 boundaries; and
84 (e) solidified metal.

85 During initial solidification in CC, the stresses in the
86 solidifying shell can be caused by both external and
87 internal origins. An important example of the latter is
88 the tensile stress due to solidification shrinkage and
89 thermal contraction within the mushy zone and in the
90 underlying solid. Being exposed to the tensile stress
91 applied perpendicular to dendrite axis—grown along
92 thermal gradient direction—the mushy zone in a poly-
93 crystalline solidifying alloy in regions (a) and (b) has
94 essentially no shear strength because of the presence of
95 interdendritic and intergranular liquid films. The den-
96 drite trunks start to pose resistance to tensile forces
97 when dendrite arms coalesce (transition b to c), trans-
98 forming continuous liquid films into isolated liquid
99 droplet within each grain. The temperature at which this
100 takes place is usually referred to as zero strength
101 temperature (ZST).^[11] However, upon the film-to-drop
102 transition at grain boundaries (from c to d) a temper-
103 ature is reached, conventionally called as *rigidity point*,
104 at which a continuous dendritic network forms through-
105 out the solid. At macroscopic level, a dramatic change in
106 the solid strength occurs; the mushy zone behaves like a
107 *coherent and rigid* solid since then and the material is
108 capable of retaining its shape and transferring stresses.
109 At microstructure level, dendrite arms from neighboring
110 grains start coalescing or *bridging* to each other (*i.e.*,
111 upper bridging temperature, $T_{b,upper}$) normally at high
112 solid fractions while there are still some liquid pockets
113 or droplets at the grain boundaries which weaken the
114 solidifying metal. The so-called bridging process contin-
115 ues until last droplets turn to solid upon further
116 cooling by lower bridging temperature ($T_{b,lower}$) beyond
117 which the solid acquires its full shear strength. However,
118 the lower bridging temperature ($T_{b,lower}$) may be well
119 below the equilibrium solidus temperature depending on
120 alloy system, solute redistribution in liquid and solid
121 phases, dendrite morphology, and grain boundary
122 energy.^[12] This would increase vulnerability of the
123 solidifying shell to hot cracking during solidification
124 because it extends the film-to-drop morphological tran-
125 sition during which the material exhibits low ductility
126 and moderate strength; and any opening in boundaries
127 induced by developed thermal strain cannot be com-
128 pensated by liquid flow due to limited permeability of
129 mushy zone in this region.^[4,5]

130 Novikov^[8] defined a vulnerable part of the solidifica-
131 tion interval (VPSI), bounded between a temperature (or
132 solid fraction) at which the stresses begin to build up and
133 the solidus temperature. Based on the above argument,
134 for a polycrystalline solidifying alloy with columnar
135 dendritic morphology, one can designate VPSI with the
136 upper and lower temperatures of the bridging process for
137 the dendritic grains. Therefore, VPSI is demarcated
138 between the rigidity point—where the material sensibly
139 develops strength and transfers force, hence the stresses
140 being built up from that moment on—and the solidus
141 temperature (equilibrium or non-equilibrium depending
142 on solidification conditions). But the question is how to

determine the rigidity point for the given alloy. Novi-
kov^[8] also suggested to measure the so-called “linear
shrinkage” (more correctly “linear contraction”) of the
alloy during solidification and set the upper boundary of
VPSI as the temperature at which the linear shrinkage (or
rather linear thermal contraction) starts.

The solidification shrinkage is the volumetric change
upon transformation from fully liquid to fully solid state
in the solidification range due to the density difference
between liquid and solid phases and the temperature
dependence of density for the constituent phases. The
linear thermal contraction in the solidification range,
being a part of the total solidification shrinkage,
commences only when a rigid skeleton of interconnected
solid phase forms throughout the shell at a temperature
known as the linear contraction onset temperature
 $T_{linear,onset}$. Above this temperature, the mushy zone
behaves like a fluid (regions a and b) and any volumetric
changes can be compensated if additional melt is
supplied by a metallic head otherwise the melt level in
the mold descends (the so-called surface sink). But in the
CC mold, because of continuous supply of the melt, the
volumetric solidification shrinkage does not appear until
 $T_{linear,onset}$ is reached, hence is not measurable. Below
 $T_{linear,onset}$, the linear contraction appears as changes in
linear dimensions of the solid shell. Therefore, one can
measure it as the displacement of casting walls with
respect to the mold. These effects were previously
demonstrated for aluminum alloys.^[7]

The temperature dependency of density causes the metal
to continue thermal contraction of the shell after solidifi-
cation completion. In addition to mechanical effects on the
solidifying shell highlighted above, the thermal contraction
results in topological changes at metal/mold interface,
which continuously and noticeably reduces heat extraction
rate across the interface. The linear contraction is reported
to be the major factor bringing about air-gap formation
that decreases the cooling rate during CC.^[13] The gap
formation, in turn, can affect shell thickness and the
microstructure formation processes.

A special method was originally proposed by Novikov^[8]
to measure the linear shrinkage/contraction and pre-
shrinkage expansion upon solidification. Its background
idea was based on simultaneous measurement of displace-
ment and temperature of the solidifying alloy under
controlled solidification conditions. This method was
further developed and applied successfully for studying
the contraction behavior of binary and commercial alu-
minum alloys during and after solidification.^[6,7]

In the case of iron and steel, major thermal contraction/
expansion studies were performed by dilatometer mea-
surements at low and medium temperatures.^[14] At higher
temperatures (austenite-to- δ -ferrite transformations up
to melting point) density measurement was adopted as a
measure of thermal expansion. Also, some theoretical
calculations and models have been reported.^[15,16]

In context of casting and solidification, attention was
mostly paid to hot mechanical testing; for example,
Instron-type hot tensile testers to assess the metal
strength during melting or solidification^[17] and sub-
merged split-chill tensile (SSCT) apparatus for the *in situ*

measurement of tensile forces during shell formation.^[18] In the latter, the effect of shrinkage of the shell can be indirectly evaluated in terms of thermal stress and crack length in solidified shell.^[19] Meng *et al.*^[20] proposed a framework to simulate the shrinkage at sub-solidus temperatures. However, the Instron-type testers require careful control of dendrite growth direction during tensile tests, whereas SSCT testers need precise control of uniform shell growth around the mold. Difficulties involved in the control result in the scatter and inaccuracy of the observed data.^[9]

Therefore, a study directly dealing with thermal contraction behavior of iron and steel during and after solidification under casting conditions would be significant. This article describes the development of an experimental technique for measuring contraction of solidifying steel, and the analysis of the contraction behavior of low-alloy steels during and after solidification. In this regard, design requirements are first reviewed, the results of the contraction measurements for two commercial steel grades are given; the correlation of contraction with solidification development and the effect of steel grade are discussed. Finally, experimental results obtained using the developed technique are applied to the analysis of crack susceptibility and sub-solidus contraction.

II. EXPERIMENTAL

Almost all designs reported in literature for measurement of linear contraction during solidification—used for low melting point alloys—consist of common features such as a casting cavity with stationary and moving walls, a cooling medium to yield high cooling rates comparable to casting conditions and simultaneous measurements of temperature and displacement.

The experimental setup used in this study for measurement of the linear contraction upon solidification is based on the idea introduced by Novikov^[8] and further developed by Eskin *et al.*,^[6,7] and is shown in

Figure 1(a). The mold is made of graphite because of its high thermal conductivity and low friction properties. The mold cavity is embedded between two T-shaped geometries at both ends of the casting, as shown in Figure 1(b); one as stationary and the other as linear moving wall whose movement is measured by a displacement sensor. Also, a thermocouple measures temperature of the solidifying metal at a reference point which is discussed below.

The solidification in the cavity should be in a manner that two solidifying sections—having initiated from the either casting ends—meet, or bridge, at the central section of the casting. In this way, the contraction of the casting is controlled by conditions at the hot spot (*i.e.*, the temperature measurement point). After bridging occurs at the hot spot ($T_{\text{linear, onset}}$), the thermal contraction of the casting manifests itself as the *linear* displacement of the moving wall, being measured by the displacement sensor.

The T-shaped geometries at both heads perform a dual thermal-mechanical function. First, due to the thinner section compared to the main cavity, the melt here solidifies faster than the rest of the mold, hence these T-shaped cavities act as freezing initiators providing the desirable solidification pattern. Second, the stationary T-head restrains the sample on its end during solidification whereas the loose T-head (*i.e.*, the moving wall) is attached to and moves with the solidifying metal as a result of sample shrinkage and contraction.

The cross section of the main cavity used in experiments is 25×10 mm with a gage length of 100 mm as shown in Figure 1(b). The dimensions of the mold were chosen according to Novikov *et al.*^[21] who showed that these dimensions made the measured property not scale-dependent.

The moving wall design and displacement measurement mechanism are essential in the contraction setup. In earlier experiments with aluminum alloys, a linear variable differential transformer (LVDT) was used to measure the displacement of the moving wall. The LVDT was attached to the moving wall from outside and aligned with the longitudinal axis of the mold as

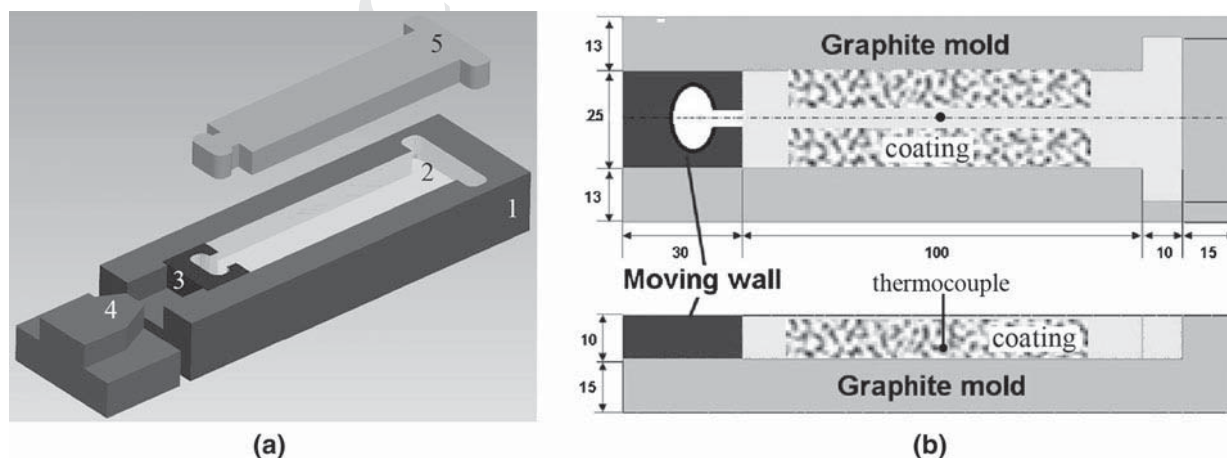


Fig. 1—Experimental setup (a): mold (1), cavity (2), moving block (3), displacement sensor (4), and casting/sample (5), and drawing of the mold and coating scheme (b) where dimensions are in mm.

reported in Reference 7. On the inner side the moving wall was connected to the sample by a threaded metallic rod. But the application of such method in the case of liquid steel, due to very high temperatures, becomes very limited. The metallic rod cannot be used for the connection due to its dissolution in the molten steel. The conduction of heat through the moving block results in intrinsic thermal expansion of connecting arm of the LVDT that brings about erroneous reading. To overcome these problems, a T-shaped cavity was made in the moving wall similar to that in the mold and a contactless laser displacement sensor was used for measurements. The linear displacement is measured by a μ -Epsilon model ILD1401-5 laser sensor, which is accurate to 3 μ m or 0.003 pct under dynamic conditions. For reproducibility of measurements within the accuracy range, each series of experimental conditions has been tested at least twice and the average values are reported. The combination of contactless displacement sensor and low friction graphite/graphite contact provides minimum impact of friction and drag on the measured contraction.

The temperature was measured by 0.35-mm-thick B-type thermocouples with an open tip that enables quick response to the changing temperature. The thermocouple is placed along centerline at central section of the cavity, close to bottom; the distance between the thermocouple tip and the bottom of the mold being about 1.5 mm. Lower distances may result in problems with filling the gap between the thermocouple tip and the mold bottom. Accuracy of temperature measurements is within 2 K (-271°C). During the experiments, the temperature and displacement are recorded simultaneously by a computerized data acquisition system (National Instrument interface and Labview software).

In addition to design considerations, heat-transfer conditions during solidification play an important role in achieving the desired freezing pattern and hence accurate and reproducible measurements. Heat transfer can be conditioned by selecting a refractory coating and its application scheme. The effect of heat-transfer conditioning on the freezing pattern was previously studied through computation and measurement of temperature distribution, using a grid of thermocouples inside the mold under different configurations, *i.e.*, bare and refractory-coated mold surfaces.^[7,22] Computer simulation of solidification of the casting in the experimental mold shows that the bridging of two almost solidified sections occurs at the central section very close to the bottom of casting.^[6,23] However, without proper mold conditioning, transverse thermal gradient due to cooling effect of side walls leads to the curvature of solidification fronts and makes the bridging at the central section happen first close to the side walls instead

of the centerline, *i.e.*, the thermocouple location. In this case, the measured temperature would not reflect the real temperature at which the contraction starts.

Therefore, the refractory coating should be applied in such a scheme that facilitates decreasing of transverse thermal gradient while increasing the longitudinal gradient and maintaining the vertical gradient for solid structure formation. If so, it is more likely to make two progressing solidification fronts flatter and meet first at the thermocouple location. Figure 1(b) depicts the optimum coating scheme in which the middle part of the mold is coated by a thick layer of zirconium oxide as a low conductivity paint. The rest of the surface of the cavity is coated by a thin layer of boron nitride as a high conductivity paint to prevent carbon pickup by the liquid steel.

Two commercial low-carbon, low-alloy steel grades used in this study were normally cast at the Direct Sheet Plant in IJmuiden, Tata Steel Mainland Europe. The chemical compositions of the alloys are given in Table I. The alloys were re-melted in an induction melting furnace under protective argon atmosphere. The liquid steel was deoxidized prior to pouring, then cast at a temperature of 1903 K (1630 $^{\circ}\text{C}$) to fill the entire mold cavity especially the gap between the thermocouple and the mold bottom. The cooling rate in the experiments was 10 to 12 K/s which is comparable to casting conditions in CC practice.

An example of the primary data, *i.e.*, temperature and displacement *vs* time, is shown in Figure 2. The cooling curve is then processed to obtain characteristic solidification temperatures and cooling rate during experiments. Also, the displacement data are reconstructed to find temperature dependency of the contraction during solidification and further cooling in solid state which is discussed in detail later. From such correlation, the linear solidification contraction, the onset temperature of linear contraction, and the linear thermal contraction coefficient (TCC) at sub-solidus temperatures can be estimated.

The linear contraction is determined as follows:

$$\varepsilon_s = [(L_s - L_i)/L_s] \times 100, \quad [1]$$

where L_s is the initial length of the sample at the measurement *start* (*i.e.*, the cavity gage length of 100 mm) and L_i is the final length of the sample corresponding to the measurement *instant*. For example, if the amount of the accumulated strain during solidification is of interest, L_i denotes the instantaneous length of the sample as the solidus temperature is reached.

Evolution of dissolved gas in the melt during solidification can result in some expansion prior to appearance of shrinkage, called pre-shrinkage expansion, which should be taken into account for calculation of the solidification

Table I. Chemical Composition of the Studied Steel Grades

Steel Grade	C (Wt Pct)	Mn (Wt Pct)	V (Wt Pct)	Nb (Wt Pct)	N (ppm)
LCAK	0.045	0.22	—	—	—
HSLA	0.045	0.8	0.13	0.013	130

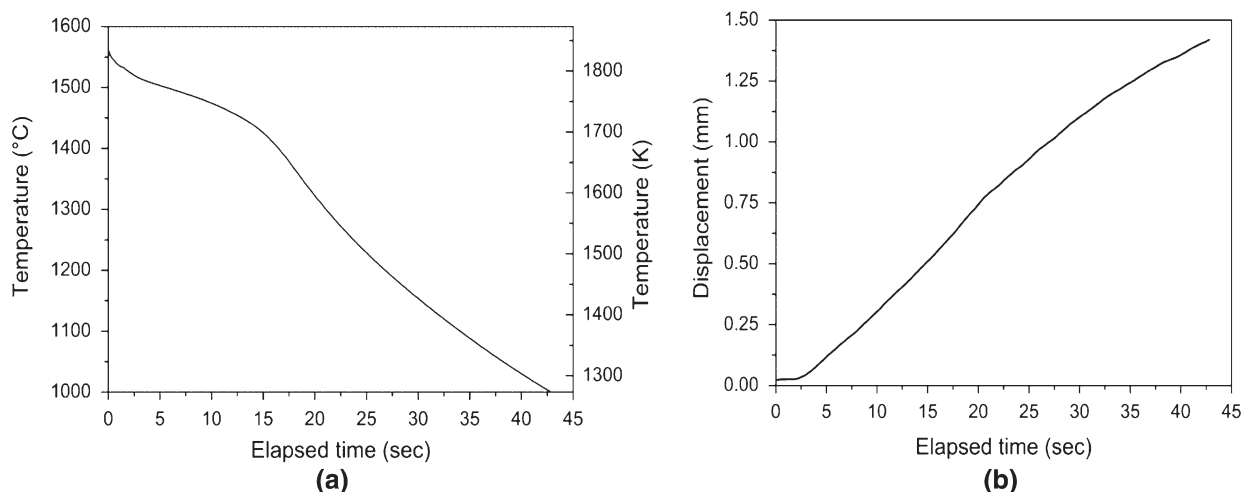


Fig. 2—Cooling curve (a) and displacement measurement (b) of HSLA-grade sample.

contraction as observed in aluminum alloy solidification.^[7,8] The occurrence of the pre-shrinkage expansion depends on alloy system, solidification conditions, and structure formation during solidification. In contrast to solidification of aluminum alloys, low-carbon steels in this study have much narrower freezing range and solidify predominantly with columnar grain morphology under CC conditions. In addition, the liquid steels in these experiments were deoxidized prior to casting. As a combination of these factors, no pre-shrinkage expansion was observed in the experiments.

The experimental materials were also analyzed using a high-temperature differential scanning calorimeter (instrument model: Setsys[®] TG DSC) to understand phase transformation sequence of the steel upon solidification and subsequent cooling as well as to determine the characteristic temperatures. The TG-DSC rod was calibrated in temperature by using a palladium standard material and measuring its melting temperature. The onset of the melting peak was determined at 1826.9 K (1553.9 °C) whereas the literature gives 1827.8 (1554.8 °C). Then, all measured temperatures on the samples curves were corrected according to the difference noticed between the measured and the literature temperatures. It has to be noticed that there is no method for the temperature calibration in the cooling mode. In fact there is always a difference between the melting temperature and the crystallization temperature for a metallic standard material due to undercooling. As a consequence the temperature calibration obtained during the heating mode was also used during the cooling mode. In addition, to calculate evolution of solid fraction during solidification under equilibrium and non-equilibrium conditions, solidification paths of the studied steel grades were simulated using ThermoCalc[®] software (database TCFE6).^[23]

III. RESULTS AND DISCUSSION

In this section, the effect of some design and processing parameters on the measurements are reviewed

first—whereby the experimental technique was improved in terms of better heat-transfer conditions, desirable freezing pattern of the sample, and correct temperature reading. After that, the contraction behavior of the studied steel grades is analyzed using the results of the experimental technique. Then, an effort is made to explain hot crack susceptibility of these steel grades based on their contraction behavior and microstructure formation during solidification. A note on the linear thermal contraction after the end of solidification is given finally.

A. Test Verification and Effect of Parameters

In practice, experimental results of the contraction measurements in the given method can be affected by a number of parameters such as the gage length of the mold, mass of the casting, dragging effects (mold friction and other opposing forces), and, particularly, heat-transfer modifiers (refractory coatings, *etc.*) inside the mold.

It was shown that the variation of the gage length from 100 to 50 mm does not affect the measured contraction.^[7] The casting mass, parameterized as height of the sample assuming the same gage length, can affect the results through altering thermal gradients, freezing pattern, and mechanical and flow properties of the solidifying metal.^[24] In this study, with decreasing level of the melt from 15 to 10 mm, the amount of contraction accumulated during solidification reduced. This would originate from inhomogeneity across a vertical section of the solidifying metal. In other words, in a thicker sample, different layers of the section are experiencing different stages of solidification; having different amounts of solid and contracting at different rates, *etc.*, which may induce additional measured contraction during solidification. Although a higher level of the melt in the experimental mold could imitate liquid metal head in CC mold, its effects would be a combination of thermal and mechanical interactions between the liquid metal and the solidifying shell. In a severe case, it can unbalance the thermal gradients

470 within the sample and affect heat-transfer conditions.
471 Therefore, for the sake of establishing more homogeneity across the sample and balanced thermal gradients, the lower metal level, 10 mm, was adopted for main tests of this study.

475 Opposing forces arising from the friction between the sliding parts of the mold can influence the measured contraction. It was reported that, for aluminum alloys, the amount of linear contraction during solidification considerably decreases as a result of such forces while the temperature of the contraction onset is not affected that much.^[6] In contrast, our experimental results show that the steel is almost insensitive to the friction effects which could be attributed to a higher strength of steel. However, low friction sliding contact, enough clearance between moving parts, and using a contactless displacement sensor are effective measures to minimize the friction and dragging effects.

8 As it is noted in Experimental, the coating should regulate heat-transfer conditions in the experimental mold so that the bridging of the almost solidified sections occurs close to the thermocouple location. Such freezing pattern can be examined through observation of the solidification structure or computer simulation. Figure 3 shows the longitudinal section of the sample through its longitudinal symmetry plane which also encompasses the thermocouple position. Figure 4 depicts the mosaic image reconstructed from tens of micrographs of the HSLA sample through the annotated section in Figure 3. Columnar dendritic structure can be clearly seen at the vicinity of mold walls under local thermal gradients. At regions far from the mold walls, the structure transits from columnar to mixed

dendrites due to decreasing thermal gradients. The solidification process can be described as follows: just after mold filling, solidification starts at the right end of the sample into strong cooling effect of T-junction and in the T-opening of the moving head, then progresses toward the central section, i.e., the left side of the micrograph in Figure 4. However, in the middle part of sample at this section, the effect of vertical thermal gradient becomes more pronounced due to bottom cooling of the mold which facilitates the primary dendrites to be aligned closer to the vertical direction. Therefore, the local thermal gradient, determining the freezing pattern and structure formation during solidification, is a combination of two parts; the vertical component along which the primary dendrites grow bottom-up and the longitudinal component which prioritizes the freezing sequence along the sample longitudinal axis so that T-heads are the first and the centerline is the last section to solidify. Such pattern causes the central section to be the hot spot of the sample. The existence of a shrinkage cavity in the central section of the sample verifies the described pattern and is in agreement with results of computer simulation of heat transfer in the experimental mold.^[6,25]

Figure 5(a) shows an idealized representation of solidification configuration around centerline based on the described freezing pattern and Figure 5(b) illustrates the observed micrograph of HSLA sample very close to the centerline where the thermocouple (TC) is located. As soon as the rigidity temperature (solid fraction) is reached in the lowermost layer of the sample, the bridging starts and the dendritic grains at either sides of the centerline coalesce together and the sample starts to retain its shape and behave like a coherent solid from that moment on. Recalling that one end of the sample is constrained and the other is fixed to the free-moving head, the thermal contraction of the solidifying metal at the hot spot results in drawing of the free, already solidified section which is attached to the moving head whose position is being registered. Therefore, the rigidity point stands for the temperature of linear contraction onset and the magnitude of the movement is a measure of the linear thermal contraction.

Notwithstanding differences in scales and spatial orientation, the solidification configuration of melt in the experimental mold in this study and the initial solidification of strand in a CC mold display several thermal, physical, and mechanical similarities. For example, the contraction of the sample in the experimental mold can simulate the free contraction of

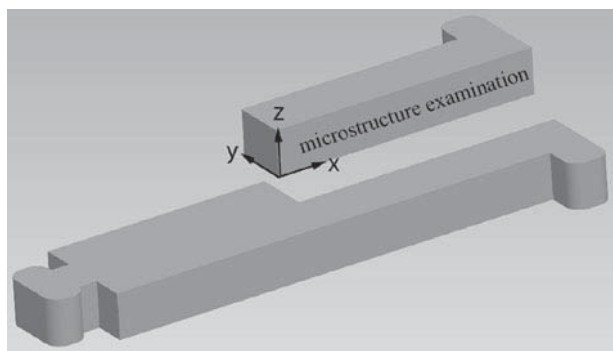


Fig. 3—Sample sectioning for micrograph examination of freezing (the coordinate system x : longitudinal, y : transverse, and z : vertical direction).

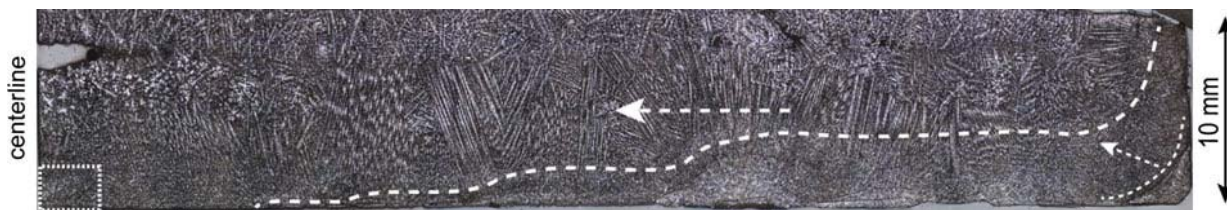


Fig. 4—The reconstructed picture of micrographs along the symmetry ($x-z$) plane of the sample shown in Fig. 3. Arrows show the freezing progression within the sample. The dotted rectangle (where thermocouple is located) is shown in Fig. 5(b).

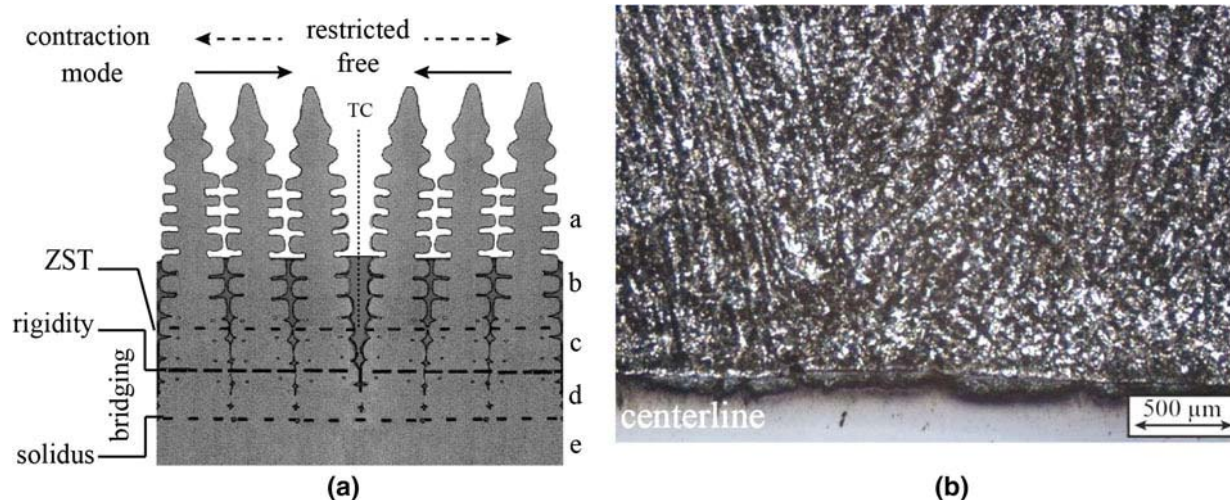


Fig. 5—Idealized representation of two (symmetric) dendritic grains with a grain boundary (a), microstructure of the HSLA sample at the vicinity of mold close to the central section (b). Properties of regions a through e are mentioned in Section 1.

solidifying shell over the wide face of a CC mold as the strand moves inside the mold along casting direction, which results in separation of the strand from the CC mold narrow faces and in the air-gap formation.^[20] The gap formation causes the rise of surface temperature and weakening of the shell with a risk for crack formation.^[1,2] To accommodate this shrinkage and contraction, the narrow faces of a CC mold are tapered.^[20] Alternatively, if thermal contraction (quantified as the corresponding thermal strain) of the solidifying shell is restricted by any means, a tensile thermal stress is developed in the shell which is applied perpendicular to the growth direction of the solid and causes the opening of the dendrites during solidification and cracking. These modes are depicted in Figure 5(a) with arrows over the dendrites.

B. Solidification Analysis

The understanding of contraction phenomena needs supplementary information about material behavior upon solidification and subsequent cooling, *i.e.*, phase transformation sequence of the alloys and evolution of the solid fraction during solidification should be known. The phase transformation sequence of the given steel grades was calculated using the ThermoCalc[®] software. To determine the transformation temperatures for conditions closer to the experimental conditions, the steel samples were analyzed using DSC with a rate of 20 K/s. The onsets of peaks on heating and on cooling were used as characteristic temperatures. Since the primary output of DSC measurement for temperature difference is in μV , this is what reported in this paper as the heat flow values were not of interest in these experiments. The lower temperature limit in this study was chosen as 1273 K (1000 °C) because the strand surface temperature exiting the CC mold is reported to be around this temperature.^[20]

Figure 6 gives examples of the calculated pseudo-binary phase diagram of a low-alloy steel system and

also the corresponding DSC results. HSLA steel, as marked off in Figure 6(a), solidifies fully in the δ -ferrite mode. Upon subsequent cooling, δ -ferrite transforms to austenite (γ) completely in the solid state and MnS precipitates at lower temperatures. To concur with that, DSC results, as shown in Figure 6(b), display typical curve of δ -ferrite solidification in the HSLA steel. The HSLA steel shows liquidus and solidus temperatures of 1801 K and 1777 K (1528 °C and 1504 °C), respectively. Similarly, LCAK-grade steel also exhibits δ -ferrite solidification mode, with 1806 K (1533 °C) liquidus and 1782 K (1509 °C) solidus temperatures, followed by δ/γ transformation upon further cooling in the solid state but with different transformation temperatures. The temperatures related to the start and end of these phase transformations for the studied steel grades are summarized in Table II based on the phase diagram calculations and the experimental measurements.

The evolution of fraction of solid, required for characterization of the linear contraction onset, was calculated using ThermoCalc[®] under two different conditions. At higher cooling rates, at which non-equilibrium effects become more important, the Scheil model was used to estimate the extreme non-equilibrium solidification conditions (the solidus temperature and the evolution of solid fraction). In practice, the solidification would occur under intermediate conditions. In the Scheil approximation, δ -ferrite was the solid phase forming during solidification and carbon and interstitial components were considered as fast-diffusing elements. The results of the calculated solid fractions in the equilibrium and Scheil solidification modes can be seen in Figure 7 for both steels. It is noteworthy that there is a slight difference in the solidification paths of the LCAK steel under two conditions supposedly due to its lower alloy content while for the HSLA steel the DSC-measured solidus is closer to the calculated temperature in the equilibrium curve.

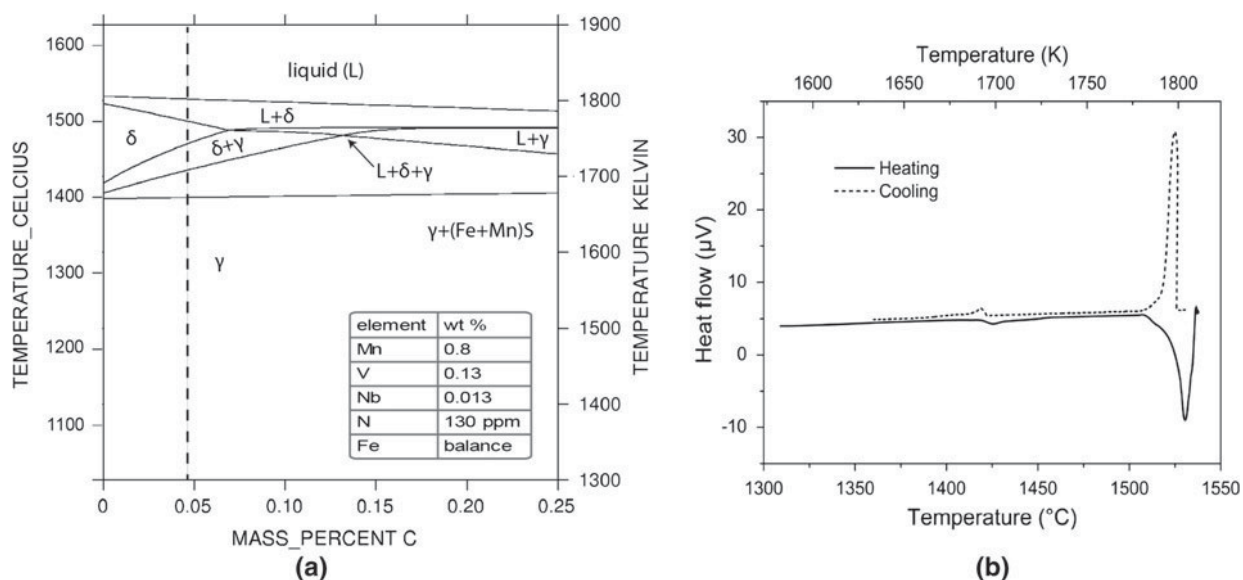


Fig. 6—Calculated phase diagram (a) of low-alloy steel of the indicated chemical composition showing transformation path of the HSLA steel (dashed line) upon solidification and cooling; the corresponding DSC measurement (b) for the HSLA steel showing δ -solidification mode and δ/γ transformation in solid.

Table II. Transformation Temperatures [K (°C)] in the Studied Steels

Transformation	HSLA Phase Diagram [K (°C)]	HSLA Experimental [K (°C)]	LCAK Phase Diagram [K (°C)]	LCAK Experimental [K (°C)]
$L \rightarrow L + \delta$	1802 (1529)	1801 (1528)	1807 (1534)	1805 (1532)
$L + \delta \rightarrow \delta$	1780 (1507)	1777 (1504)	1784 (1511)	1780 (1507)
$\delta \rightarrow \delta + \gamma$	1739 (1466)	1716 (1443)	1734 (1461)	1729 (1456)
$\delta + \gamma \rightarrow \gamma$	1706 (1433)	1691 (1418)	1702 (1429)	1697 (1424)

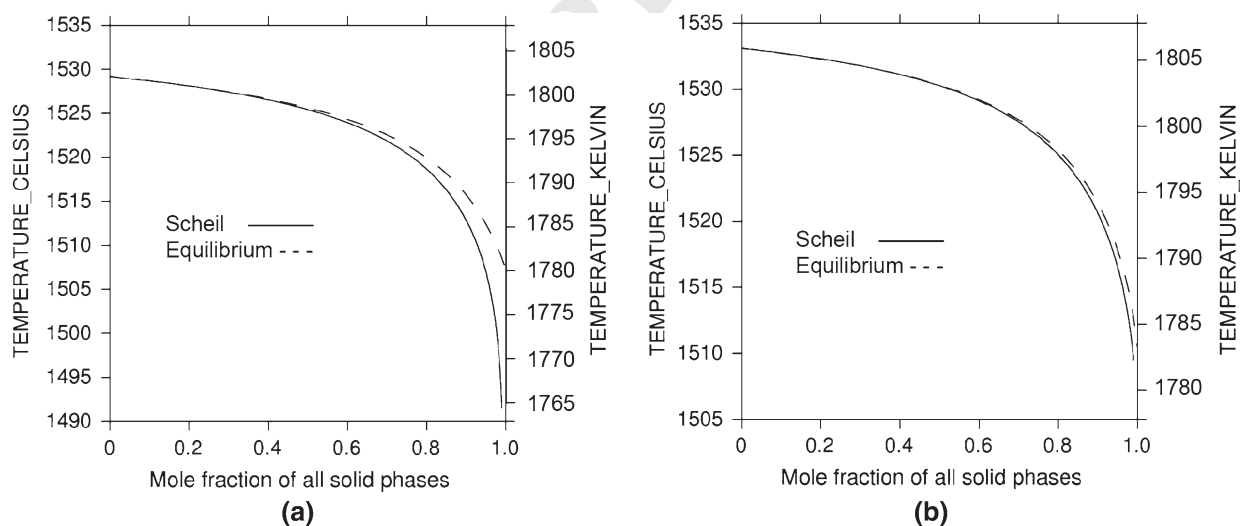


Fig. 7—Calculated evolution of solid fraction in the HSLA (a) and the LCAK steel, (b) during δ -solidification under equilibrium and Scheil conditions.

C. Thermal Contraction During Solidification

As the next step, the volumetric shrinkage occurring during solidification of δ -ferrite was calculated using volume and density change data based on measurements and model given in References 15, 16. This volume

change, mainly resulting from the density difference between liquid steel and δ -ferrite, develops over the solidification range. Total solidification shrinkage accumulated between the liquidus and the solidus for HSLA and LCAK is about 3.5 pct.

However, this average 3-D shrinkage first shows up as the decrease in melt level in the mold (surface sink) before the metal retains its rigidity and the sample can contract uniformly (linearly). Therefore, the volume solidification shrinkage is much larger than the linear thermal contraction and cannot be used for assessment of hot tearing susceptibility or geometry changes during CC.^[20] The temperature dependency of the linear contraction of the studied low-carbon and low-alloy steel is shown in Figure 8 and some selected accumulated linear contraction values are summarized in Table III. Our measurements show that the linear contraction developed upon solidification of HSLA and LCAK grades are about 0.13 and 0.18 pct, respectively. Although no relevant values have been yet reported for steel, one may consider the thermal contraction in the solidification range of an Al-Cu alloy as a benchmark. For example, during solidification of an Al-4 wt pct Cu alloy, linear contraction values of 0.16 to 0.22 pct have been reported at low friction forces while this alloy has about 5.3 pct volume contraction upon solidification.^[6]

The important parameter derived from the experimental results is the temperature at which the linear contraction starts. For the HSLA grade, the linear contraction onset temperature ($T_{\text{linear,onset}}$) is about 1790 K (1517 °C). This value is indeed a measure of temperature or solid fraction at which the bridging between the solidified sections starts and a rigid

dendritic network forms. It was pointed out for other alloy systems that this temperature is independent of the friction force and known as a characteristic temperature of an alloy.^[6] Referring to the calculated solid fraction developing during solidification of the HSLA steel (Figure 7(a)), the linear solidification contraction onset corresponds to a solid fraction of 0.83 to 0.87 depending on solidification conditions. Shin *et al.*^[26] explored the tensile strength of *in situ* solidifying Fe-(0.06 to 0.6) wt pct C-1 pct Mn steels near their solidus temperatures using Instron-type high-temperature tensile strength tester. They found that the solid fraction (f_s) at ZST for these alloys is about 0.6 to 0.8 as the fraction in which dendrite arms start to interact to resist tension. These values are close to the measured values in this investigation. The difference could be due to the fact that for a polycrystalline metal ZST is reached at higher temperature (or lower solid fraction) which is shown in Figure 5(a). It is even possible that the temperature of contraction onset lies between the temperatures of equilibrium and non-equilibrium solidus—as it is the case of most aluminum alloys—in which the bridging of dendritic network and, in turn, the rigidity happen at very high solid fractions.

It can be readily seen that HSLA and LCAK exhibit quite similar contraction behaviors because their solidification mode and phase transformation sequence are very close except that their transformation temperatures and phase compositions are different. The linear solidification contraction of the LCAK steel commences at 1801 K (1528 °C) which is higher than that of the HSLA steel, as the LCAK grade has the higher liquidus temperature. The solid fraction corresponding to the linear contraction onset of the LCAK steel is about 0.72 which is a lower value with respect to the HSLA grade. Also, the accumulated solidification contraction of the LCAK steel is 0.18 pct which is larger compared with that of the HSLA steel.

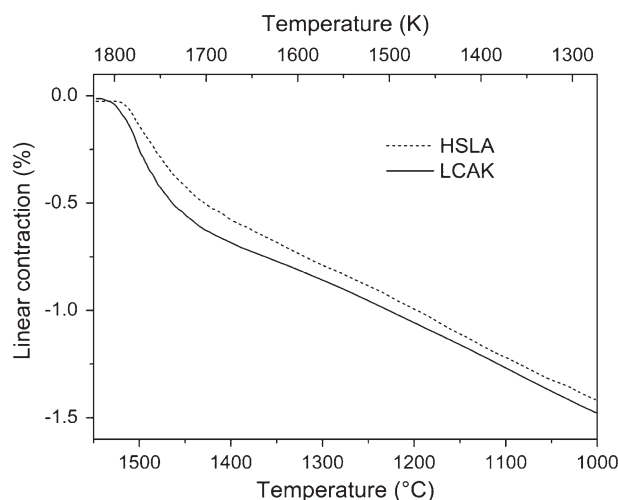


Fig. 8—Reconstructed contraction curves of the HSLA and the LCAK steel grades. Important values are summarized in Table III.

D. Steel Grade and Crack Susceptibility

Comparing the contraction data of the studied steel grades, one can find a correlation between the solid fraction and the thermal contraction as follows: the lower the solid fraction at the contraction onset temperature, the larger the accumulated thermal contraction in the solidification range. In this regard, the contraction behavior could provide a basis for the analysis of hot cracking susceptibility of these steels. Analysis of the evolution of solid fraction along with the contraction behavior reveals that although the liquidus temperature of the HSLA steel is lower than that of the

Table III. Summary of Contraction Values of the Studied Steels

Alloy	$T_{\text{linear,onset}}$ [K (°C)]	Solid Fraction ($T_{\text{linear/onset}}$)	Solidification Range	Accumulated Thermal Strain (Pct) _z Down to		
				δ/γ Transformation	1273 K (1000 °C)	γ -TCC (Average) 10^{-6} K^{-1}
HSLA	1790 (1517)	0.85	0.13	0.54	1.42	21 to 22
LCAK	1801 (1528)	0.71	0.18	0.65	1.49	20 to 21



LCAK steel by almost 5 K (-268°C), its contraction onset temperature $T_{\text{linear, onset}}$ is lower by more than 10 K (-263°C) as compared to that of LCAK which corresponds to solid fractions of 0.85 and 0.72 for the HSLA and LCAK grades, respectively. In fact, LCAK steel experienced an earlier onset of thermal contraction within solidification range and, as a result, is exposed to a greater accumulated contraction, or strain, during solidification. Therefore, one can hypothesize that a higher level of strain in the LCAK steel upon solidification can cause larger level of thermal stresses and increase its susceptibility to hot cracking as compared to the HSLA steel.

On the other hand, structure development within the mushy zone, as described in Introduction, is also a determining factor for the rigidity point and affects the contraction behavior during solidification. The solidification microstructure of these steel grades was studied in References 27, 28. Both experimental measurements and phase field simulation show coarser columnar dendritic grains associated with the LCAK grade as compared to the HSLA steel during solidification. The coarser dendritic structure leads to an earlier interaction of dendrites and their bridging at lower solid fractions. This results in the enlargement of the VPSI in which the metal is experiencing stresses with limited ductility. Such trend agrees with the experimental results in this study.

In addition, hot tensile behavior of these two alloys was also investigated using *in situ* solidification^[29] whereby zero strength and zero ductility points of the alloys have been determined experimentally. The results show that brittle temperature range for LCAK is larger than that of HSLA while its fracture mode is more brittle as compared to HSLA fracture. Plant observations of high-speed thin-slab casting of LCAK and HSLA steels along with statistical analyses of continuously cast slabs show that LCAK has yielded more defect records in terms of larger number of breakouts and cracks.^[29] So the results of tensile behavior and casting observations confirm the hypothesis of a greater hot cracking susceptibility of LCAK steel based on experimental results of the contraction study in this paper.

Similar to aluminum alloys,^[7,8] the analysis of contraction behavior during solidification of steel can be utilized as a tool to predict the hot cracking susceptibility in CC. Our results show that the temperature of the linear contraction onset is close to the temperature at which, according to reference data, the hot cracking occurs. For example, Reference 30 reported that C-Cr steel possesses negligible ductility, hence is very susceptible to hot cracks, at a solid fraction of 0.8, nearly the same value as the rigidity point determined from our contraction experiments. Therefore, the rigidity concept, the linear contraction onset temperature, and the amount of the linear contraction are of both fundamental and technical significance.

E. Thermal Contraction After Solidification

The contraction behavior of the solidified shell immediately after solidification affects not only stress

build-up within interior layers but also heat extraction process. Of special importance is δ/γ transformation during solidification and subsequent cooling. Such sequence of phase change is believed to be responsible for increasing level of defect formation and reducing heat flux during initial shell solidification and the reasons are especially attributed to volume contraction accompanying the δ/γ transformation.^[2] The magnitude of volume change upon the transformation was reported to be about 0.3 pct.^[31] In contrast to peritectic steels in which δ/γ transformation starts in the two-phase liquid-solid region and completes in the solid state,^[32] in low-carbon, low-alloy steel grades investigated in this paper, this transformation both starts and completes in the solid state and over a temperature range. So the impact of the transformation contraction on hot cracking is less pronounced here than in peritectic steels. However, the analysis of linear contraction of the just-solidified alloy during subsequent cooling can be used to explain geometrical changes of the shell below meniscus region in the CC mold.

The linear contraction is conventionally expressed in terms of linear thermal expansion or contraction coefficient—a well-known thermophysical property of the material. However, relevant reference data on the linear thermal expansion coefficients are seldom available for commercial alloys at high, sub-solidus temperatures. Moreover, those available values, usually determined by dilatometer, densitometer, lattice parameter measurements, *etc.*, as reviewed in Reference 14, are pertinent to nearly isothermal conditions using carefully homogenized samples. Efforts are even made to conduct the measurements close to equilibrium state of the alloy where removal of thermal gradients within the sample is attempted. Recalling that the real contraction conditions of a just-solidified bulk sample depart far from the equilibrium, knowledge of thermal expansion under conditions comparable to casting is required.

The developed technique can be utilized to analyze the contraction behavior of steel after solidification. The contraction of a sample at sub-solidus temperatures would be complex as different layers in the sample are undergoing different stages of solidification or cooling. The nonlinear section appearing in the sub-solidus part of the contraction curve may denote phase transformation in thermocouple location. For example, upon cooling within 1733 K to 1703 K (1460°C to 1430°C) which is the range close to δ/γ transformation (see Table II), the given steel grades contract about 0.11 pct. Assuming isotropic contraction for the solid steel and multiplying this contraction (0.11 pct) by 3 to obtain volume change, one notes that the sample undergoes 0.33 pct volume change over this temperature range which is close to 0.3 pct attributed to δ/γ transformation.^[31] Hence, such nonlinear transitions in the contraction curve can correspond to δ/γ transformation and denote a correlation between phase transformation and contraction behavior of the material. Although direct estimation of the TCC from the contraction curve is not straightforward within the transitory part, the magnitude of accumulated contraction over the extended phase change interval (including both solidification and

solid δ/γ transformation) would be a measure of geometric changes of the solidifying shell just below meniscus. Accordingly, HSLA steel undergoes about 0.54 pct linear contraction upon δ -ferrite solidification and transformation to γ -phase while LCAK experiences about 0.65 pct, *i.e.*, a larger linear contraction upon the extended phase change interval (see Table III).

The linear TCC of γ -phase, corresponding to the linear part of contraction curve, can be readily estimated by slope of the displacement curve according to TCC definition.^[33] Alternatively, the average TCC can be calculated by

$$TCC = [(L_{T2} - L_{T1})/L_{\text{gage}}]/(T_2 - T_1), \quad [2]$$

where T_2 and T_1 are the temperatures below the solidus; L_{T2} and L_{T1} are the positions read by the displacement sensor at T_2 and T_1 , respectively; and L_{gage} is the gage length of the sample. For HSLA steel, average value of 21 to $22 \times 10^{-6} \text{ K}^{-1}$ was obtained for TCC in γ -phase. As also seen in Figure 8, the contraction trends of HSLA and LCAK steels in austenite phase are similar with slight difference in TCC values. In LCAK, the results show average values of 20 to $21 \times 10^{-6} \text{ K}^{-1}$ for TCC in γ -phase which is close to earlier measurements reported for ultra-low carbon (ULC) steel at the same temperature range.^[14] It follows that TCC of γ -phase of the tested low-carbon and low-alloy steels is a weak function of chemical composition. Furthermore, as the strand surface temperature at the vicinity of mold exit is about 1273 K (1000 °C), the accumulated linear thermal contraction down to this temperature would be of technical significance. Our measurements show such values of 1.42 and 1.49 pct for HSLA and LCAK, respectively. Meng *et al.*^[20] simulated the shrinkage of a 0.044 pct C steel strand (continuously cast at 1.5 m/min) during solidification and cooling within the mold region where the strand surface temperature was about 1273 K (1000 °C) upon exiting the mold. The simulation predicts an accumulated linear contraction of 1.4 pct which is very close to the measurements of this study. Therefore, this knowledge can be incorporated in computer simulation for mold design (*e.g.*, to accommodate the geometric changes of the solidifying shell) and process optimization purposes.

IV. CONCLUSIONS

1. A technique was developed for experimental studying of the contraction behavior of steel during solidification.
2. Using the developed technique, a better understanding of the contraction behavior of low-carbon low-alloy steels can be acquired during and after solidification under conditions comparable to those of CC practice. The method is capable of characterizing the contraction of the material in terms of the temperature of the contraction onset, the amount of contraction in the solidification range, and the coefficient of thermal contraction at sub-solidus temperatures.
3. A correlation can be made among the structure formation, fraction of solid corresponding to the linear

contraction onset temperature, and the amount of the contraction accumulated in the solidification range. In spite of similar contraction trend due to the similar solidification path, LCAK and HSLA steels in this study exhibit rigidity at solid fraction of 0.72 and 0.82 to 0.87, respectively. LCAK possesses a coarser dendritic structure and undergoes a larger linear contraction than HSLA during solidification.

4. Linear contraction behavior of steel during solidification could be a measure to reflect its hot cracking susceptibility. In this regard, lower solid fraction at rigidity point, larger VPSI and larger accumulated contraction during solidification could deteriorate the hot crack susceptibility of the alloy. The higher susceptibility of the studied LCAK grade, as observed to be more than that of the HSLA grade in mechanical testing and plant casting, can be explained through its contraction properties, *i.e.*, being rigid at a lower solid fraction and having a larger accumulated strain during solidification compared to the HSLA grade of steel.
5. The contraction behavior of the studied steels at sub-solidus temperatures is a complex process but quite similar for the studied steels with close values of the TCC and in agreement with literature data. The technique can be used for determining the TCC and total contraction at high temperatures under casting conditions in the primary cooling zone of CC machine, with results being suitable for computer simulation, process design, and optimization.

ACKNOWLEDGMENTS


The work is done within the framework of the research program of Materials innovation institute (www.m2i.nl), under project M41.5.08321. The authors thank Dr. B. Santillana for providing useful materials and Mr. S. Sengo for sample preparation and optical microscopy.

REFERENCES

1. A. Grill, K. Sorimachi, and J.K. Brimacombe: *Metall. Trans. B*, 1976, vol. 7B, pp. 177–89.
2. J.K. Brimacombe and K. Sorimachi: *Metall. Trans. B*, 1977, vol. 8B, pp. 489–505.
3. B.G. Thomas: *Metall. Mater. Trans. B*, 2002, vol. 33B, pp. 795–812.
4. J. Campbell: *Castings*, 2nd ed., Butterworth-Heinemann, Oxford, 2003, pp. 242–50.
5. J.A. Dantzig and M. Rappaz: *Solidification*, EPFL Press, Lausanne, 2009, pp. 358–60.
6. D. Eskine, J. Zuidema, Jr, and L. Katgerman: *Int. J. Cast Met. Res.*, 2002, vol. 14, pp. 217–24.
7. D.G. Eskin, Suyitno, J.F. Mooney, and L. Katgerman: *Metall. Mater. Trans. A*, 2004, vol. 35A, pp. 1325–35.
8. I.I. Novikov: *Goryachelomkost tsvetnykh metallov i splavov (Hot Shortness of Nonferrous Metals and Alloys)*, Nauka, Moscow, 1966.
9. T. Emi: in *The Making, Shaping and Treating of Steel: Casting Volume*, A.W. Cramb, ed., AISE Steel Foundation, Pittsburg, PA, 2003.
10. W. Kurz: *La Metallurgia Italiana*, 2008, vol. 99, pp. 56–64.



11. T. Emi: *Mechanical Properties of Steel Near Solidus Temperatures, Handbook of Iron and Steel*, ISIJ, Tokyo, Japan, 1979, pp. 217–24.
12. M. Rappaz, A. Jacot, and W.J. Boettinger: *Metall. Mater. Trans. A*, 2003, vol. 34A, pp. 467–79.
13. K.Y. Kim: *ISIJ Int.*, 2003, vol. 43, pp. 647–52.
14. Y.S. Touloukian, R.W. Powell, C.Y. Ho, and P.G. Klemens: *Thermal expansion*, Plenum, New York, 1970, pp. 157–60.
15. P. Wray: *Metall. Mater. Trans. B*, 1976, vol. 7B, pp. 639–46.
16. A. Jablonka, K. Harste, and K. Schwerdtfeger: *Steel Res.*, 1991, vol. 62, pp. 24–33.
17. E. Schmidtman and L. Pleugel: *Arch. Eisenhüttenwes*, 1980, vol. 51, pp. 49–61.
18. P. Ackermann, W. Kurz, and W. Heinemann: *Mater. Sci. Eng.*, 1985, vol. 75, pp. 79–86.
19. C. Bernhard and G. Xia: *Ironmak. Steelmak.*, 2006, vol. 33, pp. 52–56.
20. Y. Meng, C. Li, J. Parkman, and B.G. Thomas: in *Solidification Process and Microstructure*, M. Rappaz, ed., TMS, Charlotte, 2004, pp. 33–39.
21. I.I. Novikov, G.A. Korol'kov, and A.N. Yakubovich: *Russ. Cast. Prod.*, 1971, vol. 8, pp. 333–34.
22. M. M'Hamdi, A. Pilipenko, and D. Eskin: *AFS Trans.*, 2003, vol. 113, pp. 333–40.
23. ThermoCalc, <http://www.thermocalc.se>.
24. L. Zhang, D.G. Eskin, M. Lalpoor, and L. Katgerman: *Mater. Sci. Eng. A*, 2010, vol. 527, pp. 3264–70.
25. Suyitno, D.G. Eskin, and L. Katgerman: *9th Int. Conf. Alum. Alloys (ICAA9)*, Institute of Materials Engineering, Melbourne, Australia, 2004, pp. 1309–15.
26. G. Shin, T. Kajitani, T. Suzuki, and T. Umeda: *Tetsu-to-Hagane*, 1992, vol. 78, pp. 587–93.
27. B. Böttger, M. Apel, B. Santillana, and D.G. Eskin: *IOP Conf. Ser.*, 2012, vol. 33, p. 012107, DOI:10.1088/1757-899X/33/1/012107.
28. H. Mehrara, B. Santillana, D.G. Eskin, R. Boom, L. Katgerman, and G. Abbel: *IOP Conf. Ser.*, 2012, vol. 27, p. 012046, DOI:10.1088/1757-899X/27/1/012046.
29. B. Santillana, D.G. Eskin, R. Boom, and L. Katgerman: *IOP Conf. Ser.*, 2012, vol. 27, p. 012059, DOI:10.1088/1757-899X/27/1/012059.
30. H. Mizukami, A. Yamanaka, and T. Watanabe: *ISIJ Int.*, 1999, vol. 85, pp. 592–98.
31. T.W. Clyne, M. Wolf, and W. Kurz: *Metall. Trans. B*, 1982, vol. 13B, pp. 259–66.
32. P. Presoly, R. Pierer, and C. Bernhard: *IOP Conf. Ser.*, 2012, vol. 33, p. 012064, DOI:10.1088/1757-899X/33/1/012064.
33. F. Cverna: *Thermal Properties of Metals*, ASM International, Materials Park, OH, 2002, pp. 9–10.

	Journal : MMTA	Dispatch : 28-10-2013	Pages : 12
	PIPS No. : 2089	<input type="checkbox"/> LE	<input type="checkbox"/> TYPESET
	MS Code :	<input type="checkbox"/> CP	<input type="checkbox"/> DISK